Effect of boundaries on the force distributions in granular media

Jacco H. Snoeijer,[1] Martin van Hecke,[2] Ellák Somfai,[1,*] and Wim van Saarloos[1]

[1] *Instituut–Lorentz, Universiteit Leiden, Postbus 9506, 2300 RA Leiden, The Netherlands*
[2] *Kamerlingh Onnes Lab, Universiteit Leiden, Postbus 9504, 2300 RA Leiden, The Netherlands*

(Dated: February 1, 2008)

The effect of boundaries on the force distributions in granular media is illustrated by simulations of 2D packings of frictionless, Hertzian spheres. To elucidate discrepancies between experimental observations and theoretical predictions, we distinguish between the weight distribution $\mathcal{P}(w)$ measured in experiments and analyzed in the q-model, and the distribution of interparticle forces $P(f)$. The latter one is robust, while $\mathcal{P}(w)$ can be obtained once the local packing geometry and $P(f)$ are known. By manipulating the (boundary) geometry, we show that $\mathcal{P}(w)$ can be varied drastically.

PACS numbers: 45.70.-n, 45.70.Cc, 46.65.+g, 05.40.-a

A crucial property of granular materials is their heterogeneity [1]. In particular, the strong fluctuations of interparticle forces and the organization of the largest of these in tenuous force networks have recently attracted considerable attention [2, 3, 4, 5, 6, 7, 8]. The probability density function of forces is thus a basic object of study. Measurements [2, 3, 4, 5], numerical simulations [6, 7] and theory [8] agree that such force distributions decay exponentially for large forces [9]. The behavior for small forces is less well settled; while the q-model [8] seems to predict a vanishing probability, experiments and numerical simulations clearly show that this probability remains non-zero for small forces. Since the small force distribution may be a fingerprint of arching [10], or of whether a system is jammed or unjammed [11], it is important to obtain a clear physical interpretation of this discrepancy.

In this paper, we resolve this issue by elucidating the effect of the *local* packing geometry on the force network in 2D packings of frictionless, Hertzian spheres under gravity (see Fig. 1a). To do so, it is important to distinguish the effective weight W of a particle j from the interparticle forces F (Fig. 1b). In the bulk, this weight is carried by the other particles on which particle j rests; however, the particles in the bottom layer are typically supported by the bottom only, so the forces exerted on the support are then to a good approximation the same as the weights. *Thus it is essentially the distribution of weights $\mathcal{P}(W)$ which is probed in experiments* where the particle-wall forces are extracted from the imprints on carbon paper [2, 3] or by force sensors [4]. Likewise, the main prediction of the q–model is for the distribution $\mathcal{P}(W)$, rather than for the distribution of interparticle forces, denoted by $P(F)$.

For our case of frictionless spheres, we define the weights W as (see Fig. 1b)

$$W_j \equiv m_j g + \sum_{<i>} (\vec{F}_{ij})_z \ . \qquad (1)$$

Here m_j denotes mass, g denotes gravity, $\vec{F}_{ij}$ are the interparticle forces, and the sum runs over all n_c particles

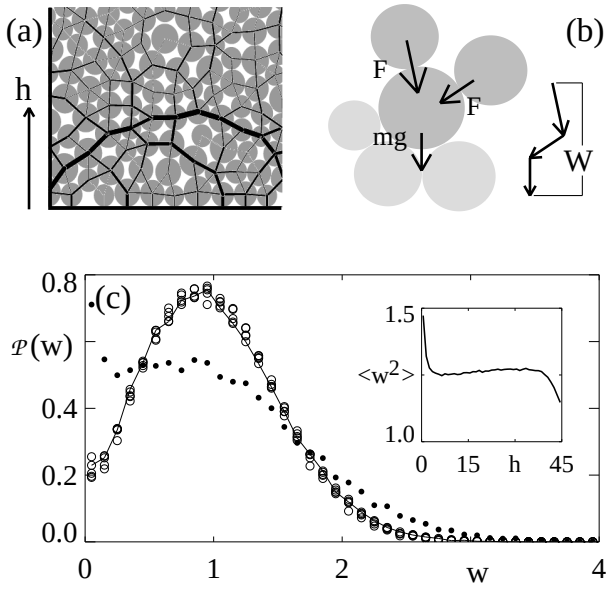

FIG. 1: (a) Detail of a typical packing and force network in our simulations; the height h denotes the distance from the bottom. (b) Definition of interparticle forces F and weight W, for a particle with $n_c = 2$. (c) The weight distribution $\mathcal{P}(w)$ at various heights between 10 and 30 in the bulk (open circles), for $2 < h < 3$ (full curve) and at the bottom (dots). Inset: The second moment $\langle w^2 \rangle$ as a function of height h.

that exert a force on particle j *from above* (see Fig. 1b). In the following we rescale W and F to their average values, and write the rescaled weights and forces as w and f, with distributions $\mathcal{P}(w)$ and $P(f)$.

Our main findings are the following: *(i)* $\mathcal{P}(w)$ changes *qualitatively* when approaching a boundary; in particular the probability of finding a small weight is much larger at the bottom than in the bulk (Fig. 1c). *(ii)* The number of contacts from above, n_c, crucially influences the distribution $\mathcal{P}(w)$, as can be anticipated from Eq. (1); the difference between bulk and bottom $\mathcal{P}(w)$'s is almost entirely due to the change in n_c caused by the change in packing near the boundary (Fig. 2). *(iii)* The force probability

distributions $P(f)$ and $P(f_z)$ show a much weaker variation when approaching the boundaries (Fig. 3). *(iv)* The distribution of n_c's near the bottom can be manipulated by, e.g., curving the boundary of a highly monodisperse packing and this can have a large effect on $\mathcal{P}(w)$ (Fig. 4).

Numerical method Our 2D packings consist of frictionless particles under gravity; the particles interact through normal Hertzian forces, where $f \propto d^{3/2}$ and d denotes the overlap distance [12]. Unless noted otherwise, the material constants and gravity are chosen such that a particle deforms 0.1% under its own weight, and the particle radii are drawn from a flat distribution between $0.4 < r < 0.6$. Masses are proportional to the radii cubed. The container has a width of 24, employs periodic boundary conditions in the horizontal direction and has a bottom consisting of a fixed hard support. The data shown in this paper were obtained from 1100 realizations containing 1180 particles each. We construct our stationary packings by letting the particles relax from a gas-like state by introducing a dissipative force that acts whenever the overlap distance d is nonzero.

Distribution of weights In Fig. 1c we show the weight distribution $\mathcal{P}(w)$ for the bottom particles (dots) which differs qualitatively from the bulk distributions (open circles). Moreover, we observe that the transition is remarkably sharp: in the slice $2 < h < 3$, the weight distribution is already bulk-like (full curve). In the inset of Fig. 1c we plot $\langle w^2 \rangle$ which quantifies the width of $\mathcal{P}(w)$ as a function of height h. The sharp transition of $\mathcal{P}(w)$ near the bottom is clearly visible. Additionally, in the bulk, $\langle w^2 \rangle$ slowly increases with height, due to the deformations of the particles; this effect disappears for harder particles [13]. Finally, near the top layer $\mathcal{P}(w)$ becomes sharply peaked and $\langle w^2 \rangle$ decreases.

To understand the change of $\mathcal{P}(w)$ near the bottom, consider the typical packing of Fig. 2a. The support aligns the bottom row of particles and thus strongly affects the directions of the interparticle forces. The forces between neighboring bottom particles are almost purely horizontal, so these hardly contribute to either the force on the particle from above [the "weight" in (1)] or to the force needed to support it. This approximation becomes better the smaller the polydispersity is. Thus, the average value of n_c, the number of particles that press on the particle from above and hence contribute to its weight, is on average lower at the bottom than in the bulk. Intuitively it is clear that *the probability of finding a small value of w increases with smaller n_c* for nontensile forces. This statement can be made precise by considering Eq. (1) for fixed n_c and analyzing $\mathcal{P}_{n_c}(w)$, the weight probabilities restricted to particles of given n_c. As long as the joint probability distribution of the interparticle forces remains finite for small forces, it follows from a phase-space argument that

$$\mathcal{P}_{n_c}(w) \propto w^{n_c-1} \qquad \text{for} \quad w \to 0 \ , \tag{2}$$

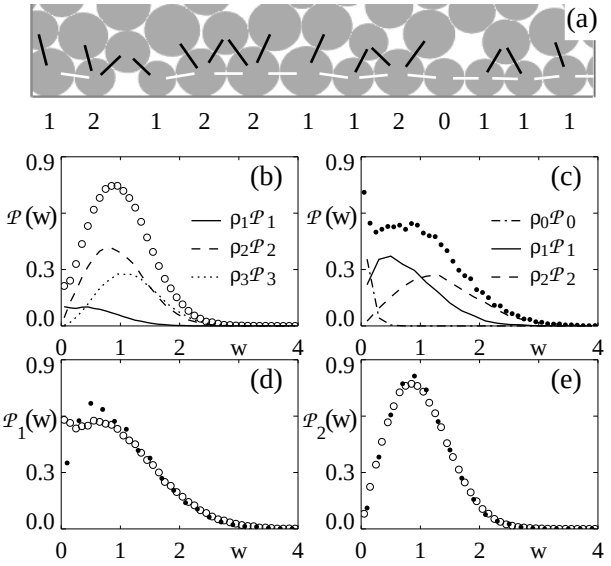

FIG. 2: (a) Detail of a typical packing, showing the dominance, near the bottom, of layer-to-layer forces (black lines) to intralayer forces (white lines) in determining w. The numbers show the values of n_c for the respective bottom particles. (b,c) Decomposition of $\mathcal{P}(w)$ according to Eq. (3) in the bulk (b) and at the bottom (c); The measured bulk values for the fractions $\{\rho_0, \rho_1, \rho_2, \rho_3\}$ in Eq. (3) are $\{0.01, 0.11, 0.52, 0.36\}$, and the bottom values are $\{0.08, 0.46, 0.44, 0.02\}$; at the bottom, we excluded the intralayer, almost horizontal forces. (d,e) When rescaled to the average value for each distribution function, $\mathcal{P}_1(w)$ (d) and $\mathcal{P}_2(w)$ (e) are essentially the same in the bulk (open circles) and at the bottom (dots).

for all $n_c \geq 1$. The particles which do not feel a force from above, $n_c = 0$, give a δ–like contribution at $W = 1$; for deep layers this occurs for $w \ll 1$.

To check the validity of this idea, we have determined $\mathcal{P}_{n_c}(w)$ both in the bulk and near the bottom by determining n_c for each particle and decomposing the weight distribution $\mathcal{P}(w)$ into the $\mathcal{P}_{n_c}(w)$'s,

$$\mathcal{P}(w) = \sum_{n_c} \rho_{n_c} \mathcal{P}_{n_c}(w) \ . \tag{3}$$

The crucial difference between bottom and bulk are the *fractions* ρ_{n_c} of particles that feel n_c other particles pressing on them from above. This can be seen in Figs. 2b-c, where we show the decomposition of $\mathcal{P}(w)$ according to Eq. (3). This picture is also confirmed by Figs. 2d-e, which show that the individual distribution functions $\mathcal{P}_1(w)$ and $\mathcal{P}_2(w)$ do not differ significantly between bulk and bottom (to compare these, we have to normalize them not to the total average weight in each layer, but to the average weight of the particles with the same n_c). Note also that Figs. 2b-e show that Eq. (2) is valid, *except for $\mathcal{P}_1(w)$ at the bottom for small values of w*; this deviation comes from neglecting the intralayer, "almost horizontal" forces, whose small vertical components eventually make $\mathcal{P}_1(w) \to 0$ for very small weights.

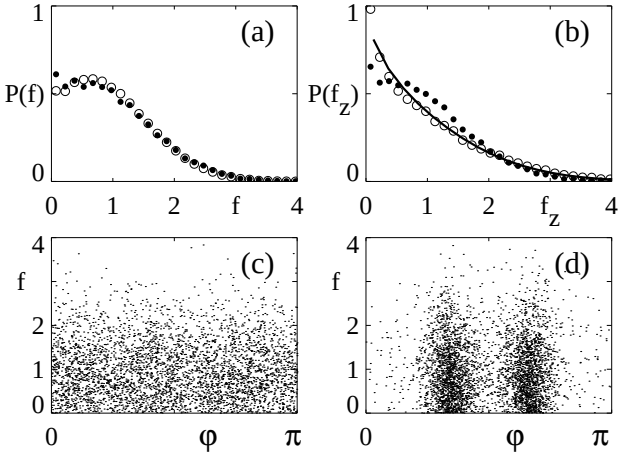

FIG. 3: (a) $P(f)$ in the bulk (open circles) and for the layer–to–layer forces (see Fig. 2a) near the bottom (dots). (b) $P(f_z)$ in the bulk (open circles) and for the layer–to–layer forces near the bottom (dots). The solid line is obtained by integrating $P(f)$ over all angles (see text). (c,d) Scatter plot of (f_{ij}, φ_{ij}) for (c) the bulk forces and (d) the layer–to–layer forces near the bottom. Same packings as for Figs. 1 and 2.

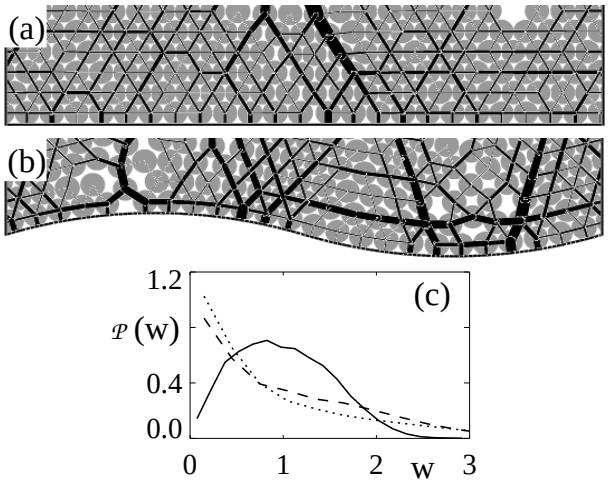

FIG. 4: (a,b) Packing and force networks in a weakly polydisperse packing near a flat bottom (a) and a curved bottom (b). (c) Distribution of weights $\mathcal{P}(w)$ on the flat bottom (solid line), convex curved bottom (dashed line) and the concave curved bottom (dotted line). The various shapes originate from the corresponding $\{\rho_0, \rho_1, \rho_2\}$: $\{0.00, 0.10, 0.90\}$, $\{0.02, 0.39, 0.58\}$ and $\{0.04, 0.46, 0.50\}$ respectively.

Interparticle forces The distributions of the interparticle forces are much more robust than the weight distributions. The results for the distribution $P(f)$ of $|\vec{f}|$ are shown in Fig. 3a. The only difference between bulk and bottom distributions is that the small *peak* around $f = 0.7$ for bulk forces becomes a *plateau* for $P(f)$ for the forces close to the bottom (see Fig. 2a). It is intriguing to note that this change from a plateau to a peak is reminiscent of what is proposed as an identification of the *jamming* transition [11].

We also have measured the distribution of angles φ_{ij}, which define the orientation of the $\vec{f}_{ij}$, and find that these angles are uniformly distributed and independent of the absolute value of $\vec{f}$ in the bulk, see Fig. 3c. Thus, in the bulk our packing is isotropic. Near the boundary, however, this isotropy is broken strongly: in agreement with our scenario for the influence of the packing geometry, the angles of the forces between bottom particles and those in the layer above are concentrated around $\pi/3$ and $2\pi/3$, as Figs. 2a and 3d show. Near the bottom, therefore, the interparticle forces naturally divide up into almost horizontal intralayer forces and "layer-to-layer" forces.

Since the weight distribution is determined by the z-components of the forces, let us also investigate the distribution $P(f_z)$. According to Fig. 3b, $P(f_z)$ also remains non-zero for small f_z, both in the bulk and near the bottom. There is a substantial difference, however, associated with the difference in packing. In the bulk, we have seen in Fig. 3c that there is no noticeable correlation between the angles φ_{ij} and the force strength f_{ij}. Hence in the bulk $P(f_z) \approx \int d\varphi df\ P(f)P(\varphi)\ \delta(f_z - f sin(\varphi))$ with $P(\varphi) = const.$ Indeed, the distribution obtained by numerical integration of this relation with $P(f)$ from Fig. 3a and a uniform angle distribution yields the solid line in Fig. 3b, which closely follows $P(f_z)$ as measured in the bulk. Near the bottom, on the other hand, the value of $\sin(\varphi)$ is concentrated around $\frac{1}{2}\sqrt{3} \approx 0.866$: in the approximation that the distribution of $\sin(\varphi)$ is sharply peaked at this value, the shape of $P(f_z)$ is close to that of $P(f)$, which is confirmed by direct comparison of the dotted datasets of panels a and b of Fig. 3.

Manipulating $\mathcal{P}(w)$ In the previous paragraphs we have shown that the weight distribution $\mathcal{P}(w)$ is very sensitive to the local packing geometry, while the distribution of interparticle forces is robust. This allows one to manipulate $\mathcal{P}(w)$ at the bottom by changing the boundary conditions. We illustrate this by simulations of weakly polydisperse particles, $0.49 < r < 0.51$, both with a flat bottom (Fig. 4a) and a *curved* bottom, consisting of two circle segments of radius 20 glued together (Fig. 4b). For the flat bottom, the particles form an almost perfect hexagonal packing, leading to particles with mostly $n_c = 2$ (horizontal contacts again not included). In agreement with (2), $\mathcal{P}(w)$ increases linearly for small w in this case. The weakly curved bottom locally disturbs this crystalline structure (Fig. 4b), causing a dramatic change in the fractions ρ_{n_c}, and correspondingly in $\mathcal{P}(w)$ (Fig. 4c). Note that the small difference between the distributions of the convex and the concave part of the bottom are reflected in the ρ_n as well. Interestingly, $P(f)$ is in all these cases indistinguishable from $P(f)$ in the strongly polydisperse case [13].

Perspective The message that emerges naturally from the above analysis is clear: in experiments in which the forces on a boundary are probed, one measures effectively

the weights w. These weights, however, are not the most fundamental quantities of a granular packing, as they are derived from the *interparticle forces* $\vec{f}_{ij}$. These capture the full microscopic structure, and the distribution function $P(f)$ of the force *strength* is quite insensitive to the packing, in contrast to $\mathcal{P}(w)$. Simple phase space considerations show that a grain with n_c contacts with particles that press downwards on it makes a contribution to the weight distribution $\mathcal{P}(w)$ which scales as w^{n_c-1} as $w \to 0$. Thus, the small weight distribution is dominated by particles with few such contacts, in particular by those with just one, and the change in geometry near boundaries leads to an atypical $\mathcal{P}(w)$. In addition, we occasionally observe a small peak at $w \ll 1$ due to "loose" particles ($n_c = 0$) which do not feel a force from above; there are indications for such a peak of $\mathcal{P}(w)$ at $w = 0$ in recent precise experiments (see Fig. 5 of [3]).

In the standard q-model, weights are randomly distributed over a fixed number of neighbors one layer below; in the simplest version there are two such neighbors that receive a fraction q and $1-q$ of the weight [8]. Due to a fixed connectivity, this model cannot be expected to capture the behavior of $\mathcal{P}(w)$, especially near boundaries. The *product* of the weight w and q, however, could be interpreted as an interparticle force. Interestingly, in the simplest case of a uniform probability distribution of the q's, the probability distribution $P(qw)$ is a pure exponential [13, 14]. In simulations of the q-model with random connectivities, a variety of $\mathcal{P}(w)$'s can be obtained, similar to what we found here for the frictionless spheres [13].

It is possible to test our framework in experiments. For $\mathcal{P}(w)$ we expect that curvature effects, such as shown in Fig. 4, only play a role when they break highly ordered packings; indeed carbon-paper measurements at the sidewalls in cylinders give a very similar $\mathcal{P}(w)$ as near the bottom [2]. A simpler way to change the boundary conditions may be to include a layer of larger particles at the boundary; their value of n_c will be higher, and we expect that $\mathcal{P}(w)$ for small w will decrease for larger n_c. Furthermore, there is a strong need of direct determination of $P(f)$, both in the bulk and near the boundaries, since the present data concerns $\mathcal{P}(w)$ only [2, 3, 4]. An interesting observation in the context of "jamming" [11] is that in our simulations the peak in $P(f)$ appears to vanish near the boundaries (Fig. 3a); are granular materials no longer jammed here, and is this relevant for the localization of shear bands near boundaries?

An important issue for future study is clearly the role of friction and dimensionality. Our numerical study has been done in two dimensions with frictionless spheres; however, recent studies indicate [7] that the coordination number for 3D packings with friction is similar to those of 2D frictionless packings. Qualitatively, the picture we have advanced is therefore expected to capture the realistic case of three dimensions with friction, because our phase space arguments are independent of dimension.

We finally note an interesting open issue. In the q-model, $\mathcal{P}(w)$ approaches its asymptotic expression as a function of depth algebraically slow [14]). In our packings, the convergence appears to be much faster — is this a real discrepancy and if so is it related with the same packing issues?

We are grateful to Martin Howard and Hans van Leeuwen for numerous illuminating discussions.

* Present address: Department of Physics, University of Warwick, Coventry CV4 7AL, U.K.

[1] H. M. Jaeger, S. R. Nagel and R. P. Behringer, Rev. Mod. Phys. **68**, 1259 (1996); P. G. de Gennes, Rev. Mod. Phys. **71**, 374 (1999); L. P. Kadanoff, Rev. Mod. Phys. **71**, 435 (1999).

[2] D. M. Mueth, H. M. Jaeger and S. R. Nagel, Phys. Rev. E **57**, 3164 (1998).

[3] D. L. Blair, N. W. Mueggenburg, A. H. Marshall, H. M. Jaeger and S. R. Nagel, Phys. Rev. E **63**, 041304 (2001).

[4] G. Løvoll, K. J. Måløy and E. G. Flekkøy, Phys. Rev. E **60**, 5872 (1999).

[5] D. Howell, R.P. Behringer and C. Veje, Phys. Rev. Lett. **82**, 5241 (1999).

[6] F. Radjai, M. Jean, J. J. Moreau and S. Roux, Phys. Rev. Lett. **77**, 274 (1996); S. Luding, Phys. Rev. E **55**, 4720 (1997); F. Radjai, D. E. Wolf, M. Jean and J. J. Moreau, Phys. Rev. Lett. **80**, 61 (1998); A. V. Tkachenko and T. A. Witten, Phys. Rev. E **62**, 2510 (2000); S. J. Antony, Phys. Rev. E **63**, 011302 (2000); C. S. O'Hern, S. A. Langer, A. J. Liu and S. R. Nagel, Phys. Rev. Lett. **88**, 075507 (2002).

[7] H. A. Makse, D. L. Johnson, L. M. Schwartz, Phys. Rev. Lett. **84**, 4160 (2000).

[8] C. Liu, S. R. Nagel, D. A. Schecter, S. N. Coppersmith, S. Majumdar, O. Narayan and T. A. Witten, Science **269**, 513 (1995); S. N. Coppersmith, C. Liu, S. Majumdar, O. Narayan and T. A. Witten, Phys. Rev. E **53**, 4673 (1996).

[9] This tail is only exponential provided that the deformations of the particles are sufficiently small [7].

[10] P. Claudin, J. P. Bouchaud, M. E. Cates and J. P. Wittmer, Phys Rev. E **57**, 4441 (1998).

[11] A. J. Liu and S. R. Nagel, Nature **396**, 21 (1998); C. S. O'Hern, S. A. Langer, A. J. Liu and S. R. Nagel, Phys. Rev. Lett. **86**, 111 (2001); I. K. Ono, C. S. O'Hern, S. A. Langer, A. J. Liu and S. R. Nagel, cond-mat/0110276 (2001).

[12] *Contact Mechanics*, by K. L. Johnson (Cambridge University Press, Cambridge, England 1985).

[13] J. H. Snoeijer *et al.* in preparation.

[14] J. H. Snoeijer and J. M. J. van Leeuwen, cond-mat/0110230 (2001); cond-mat/0202120 (2002).